AIDA-2020-PUB-2016-012

AIDA-2020

Advanced European Infrastructures for Detectors at Accelerators

Journal Publication

Luminescence rise time in self-activated PbWO4 and Ce-doped Gd3Al2Ga3O12 scintillation crystals

E. Auffray (CERN) *et al*

14 August 2016

The AIDA-2020 Advanced European Infrastructures for Detectors at Accelerators project has received funding from the European Union's Horizon 2020 Research and Innovation programme under Grant Agreement no. 654168.

This work is part of AIDA-2020 Work Package **14: Infrastructure for advanced calorimeters**.

The electronic version of this AIDA-2020 Publication is available via the AIDA-2020 web site <http://aida2020.web.cern.ch> or on the CERN Document Server at the following URL: <http://cds.cern.ch/search?p=AIDA-2020-PUB-2016-012>

Luminescence rise time in self-activated $PbWO_4$ and Ce-doped $Gd_3Al_2Ga_3O_{12}$ scintillation crystals

E. Auffray[a], R. Augulis[b], A. Borisevich[c], V. Gulbinas[b], A. Fedorov[c], M. Korjik[c], M.T. Lucchini[a], V. Mechinsky[c], S. Nargelas[d], E. Songaila[b], G. Tamulaitis[d], A. Vaitkevičius[d*], S. Zazubovich[e]

[a] CERN, Geneva, Switzerland

[b] Center for Physical Sciences and Technology, Savanorių av. 231, Vilnius, Lithuania

[c] Research Institute for Nuclear Problems, Bobruiskaya str. 11, Minsk, Belarus

[d] Vilnius University, Universiteto str. 3, Vilnius , Lithuania

[e] Institute of Physics, University of Tartu, W. Ostwaldi Str. 1, Tartu, Estonia

[*]-Corresponding author: E-mail: augustas.vaitkevicius@ff.vu.lt, Phone: +370 52366070

Highlights:

- Photoluminescence rise time is studied in two scintillators: PWO and GAGG:Ce
- Sub-picosecond photoluminescence rise time in PWO is observed for the first time
- A multicomponent luminescence rise edge is observed in GAGG:Ce
- The mechanisms behind luminescence kinetics in the crystals are under discussion

Keywords: Scintillator, luminescence, luminescence kinetics, radiation detector, lead tungstate, garnet

Abstract

The time resolution of scintillation detectors of ionizing radiation is one of the key parameters sought for in the current and future high-energy physics experiments. This study is encouraged by the necessity to find novel detection methods enabling a sub-10-ps time resolution in scintillation detectors and is focused on the exploitation of fast luminescence rise front. Time-resolved photoluminescence (PL) spectroscopy and thermally stimulated luminescence techniques have been used to study two promising scintillators: self-activated lead tungstate (PWO, $PbWO_4$) and Ce-doped gadolinium aluminum gallium garnet (GAGG, $Gd_3Al_2Ga_3O_{12}$). A sub-picosecond PL rise time is observed in PWO, while longer processes in the PL response in GAGG:Ce are detected and studied. The mechanisms responsible for the PL rise time in self-activated and doped scintillators are under discussion.

1. Introduction

Scintillation detectors are the key instrument in many fields of high-energy physics, medical diagnostic devices, tools for inspection. Currently, operation speed steps forward as the most problematic property of the scintillation detectors in many applications. Faster detector response is seeked for in high-energy physics to prevent pile-up effect in high-luminosity experiments [1-2]. Faster readout improves the signal to noise ratio and, therefore, allows a decrease of the injected dose to the patient to accumulate sufficient information in positron emission tomography (PET) [3], positron annihilation lifetime spectroscopy (PALS) [4], and other scintillator-based medical devices. Time resolution of ~200 ps is reported for detectors based on LYSO:Ce [5] and PWO with readout using avalanche photodiodes [6]. Sub-100-ps coincidence time resolution for PET with LSO:Ce codoped with Ca is reported [7]. The recent progress in development of photo-detectors, especially of silicon photomultipliers (SiPM) [8], pushes the readout rate to the frontiers limited by the kinetic parameters of the scintillation. Therefore, it is an important question whether the rise time of scintillation will be the factor hindering the targeted time resolution by a factor of ten better than currently achieved.

The scintillation is basically the luminescence in transparent media initiated by ionizing radiation [9]. Thus, the rise time of the emission is governed mainly by the excitation relaxation and the transfer of the nonequilibrium carriers to the centers of radiative recombination. Moreover, free carrier capture centers might additionally delay the population of luminescent centers. The rise time of scintillation

development might be exploited for substantial shifting the time resolution to picosecond and sub-picosecond domain [10], as seeked for in many future applications. One of the novel approaches to substantially improve the time resolution is splitting the detection into the readout of the moment of irradiation interaction with the scintillator to ensure high time resolution and the readout of the amplitude of the scintillator response carrying information on the deposited energy of ionizing radiation (see [11] and references therein).

In this paper, we present the results of our study of the rise time in two scintillating materials: self-activated led tungstate ($PbWO_4$, PWO) and Ce-doped gadolinium aluminum gallium garnet ($Gd_3Al_2Ga_3O_{12}$:Ce, GAGG:Ce).

Lead tungstate is a self-activated scintillator with predominant emission of quenched polaronic states, which can be considered as excitations on the host oxy-anionic complexes WO_4^{2-} [12,13]. In spite of a comparatively low light yield (e.g. by two orders of magnitude lower than that in LYSO:Ce) PWO has a good radiation hardness to γ-quanta and exhibits a short emission decay time, which is of especial importance to avoid the signal pile up in high luminosity experiments [14]. PWO-based radiation detectors are currently being exploited in several high-energy physics experiments, including such large experiments as CMS and ALICE at LHC [1]. The self-activated emission mechanism is expected to be favourable for fast relaxation of the nonequilibrium carriers into the emitting state.

The second crystal under study is a cerium-doped scintillator GAGG:Ce. The crystal exhibits a high light yield of up to 50000 phot/MeV, has a short luminescence decay time (less than 100 ns) [15,16], and its emission band is peaked at ~540 nm perfectly matching the sensitivity spectrum of conventional SiPMs. Thus, this crystal might compete with LYSO:Ce and LSO:Ce in TOF-PETs and other applications. However, due to the considerably different ionic radii of Ga^{3+} and Al^{3+} in both octahedral and tetrahedral oxygen coordination, the compound of gadolinium garnets of gallium and aluminum should contain a higher density of structural defects with respect to that of single-component garnets. Introduction of a gallium ion in close proximity of an aluminum ion or vice versa results in considerable lattice strain and, as a consequence, leads to distortion of the polyhedra, which serve as trapping centers for nonequilibrium carriers. This feature has been confirmed by observation of the broadening of XRD lines in mixed gallium-gadolinium garnets [17]. Moreover, the

distribution of gallium and aluminum in these garnets is random, leading to structure inhomogeneities, which significantly affect the processes of energy transfer and relaxation of electronic excitations. Therefore, the GAGG crystal has several different lattice positions for the trivalent dopant ions and exhibits significant inhomogeneous broadening in the absorption and emission spectra. These inhomogenities are being exploited for the generation of ultra-short laser pulses enabled by inhomogeneous broadening of spectral lines 4f and 3d of the activator ion, which is peculiar of the mixed garnets and is absent in single component garnets [18]. Therefore, substantial influence of structural defects on the spectra and other properties of luminescence in $Gd_3Al_2Ga_3O_{12}$:Ce is expected.

Time-resolved luminescence spectroscopy was exploited in the current study of the rise time of luminescence after short-pulse photoexcitation. To get a better understanding of the dynamics of nonequilibrium carriers generated by irradiation, the luminescence decay in these materials was also investigated, while the thermally stimulated luminescence characteristics were studied to get information on defect centers in GAGG:Ce.

2. Experimental

The PWO crystal under study was grown by Czochralski technique as described in more detail in [12]. The 2x2x0.1 cm^3 sample was prepared from the ingot of PWO-II [6] quality. The polished 2x2 cm^2 planes were perpendicular to the crystallographic axis **a.**

GAGG:Ce crystal was grown by Czochralski method in a slightly oxidized neutral atmosphere with 1 at.% Ce content in the melt. The sample under study with dimensions 0.7x0.7x0.5 cm^3 was cut from the seed part of the ingot exhibiting higher optical quality.

The time-resolved photoluminescence (TRPL) study has been performed by using a femtosecond Yb:KGW oscillator (Light Conversion Ltd.) emitting at 1030 nm. The oscillator produced 80 fs pulses at 76 MHz repetition rate. A harmonics generator (HIRO, Light Conversion Ltd.) was used to produce the third 343 nm (3.64 eV) and fourth 254 nm (4.9 eV) harmonics of the oscillator emission. The excitation beam was focused on the sample surface into a spot of ~100 μm in diameter, resulting in excitation pulse energy density of about 15 mJ/cm^2. The PL signal was detected using

a Hamamatsu streak camera. Synchoscan detection mode with the 2.95 ps full-width at half maximum (FWHM) of instrumental response function was used for the measurements in subnanosecond time domain. The deconvolution of the instrumental response function and the PL signal enabled a subpicosecond resolution. Meanwhile, in the study of samples with significant long decay components, the camera could be operated only in single sweep mode with considerably poorer time resolution.

Photoluminescence measurements were performed at room temperature, which is a typical operation temperature of ionizing radiation detectors in laboratory conditions.

The steady-state emission and excitation spectra and the characteristics of the thermally stimulated luminescence (TSL) were measured using a setup consisting of the LOT-ORIEL xenon lamp (150 W) and two monochromators (SF-4 and SPM-1). The luminescence was detected by a photomultiplier tube FEU-79 connected with an amplifier and recorder. The TSL glow curves $I_{TSL}(T)$ were measured at a heating rate of 0.2 K/s after selective irradiation of the crystal at different irradiation temperatures T_{irr} in the range from 94 to 300 K with different irradiation photon energies E_{irr} (2.2 - 4.8 eV). The crystals located in the nitrogen cryostat were irradiated with the xenon lamp through a monochromator. The spectral width of the monochromated light did not exceed 5 nm. The emission wavelength to be detected (E_{em} = 2.25 eV) was selected by the second monochromator. The TSL glow curves were not corrected for the temperature dependence of the emission intensity.

3. Experimental Results

3.1 Kinetics of photoluminescence in PWO

Figure 1 shows a typical image of the photoluminescence intensity dependence on time and wavelength, which was obtained with the streak camera for the PWO sample under study.

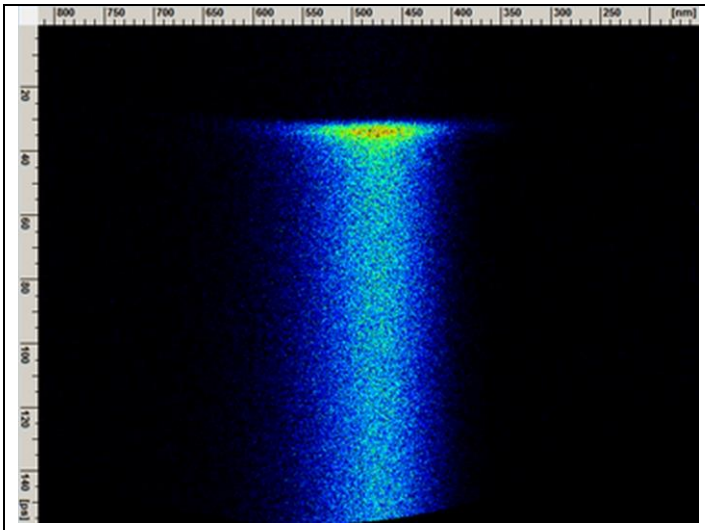

Fig. 1. Streak camera image of PL intensity versus wavelength (horizontal) and time (vertical) in $PbWO_4$. Color version available online.

Figure 2 shows the time-integrated PWO fluorescence spectra, measured at different excitation wavelengths. At the excitation into conduction band at 254 nm, the typical PWO blue luminescence is observed. For the excitation wavelength shifted to 343 nm, the green luminescence band due to recombination at oxygen deficient oxy-anionic complexes WO_3 [12] is also observed.

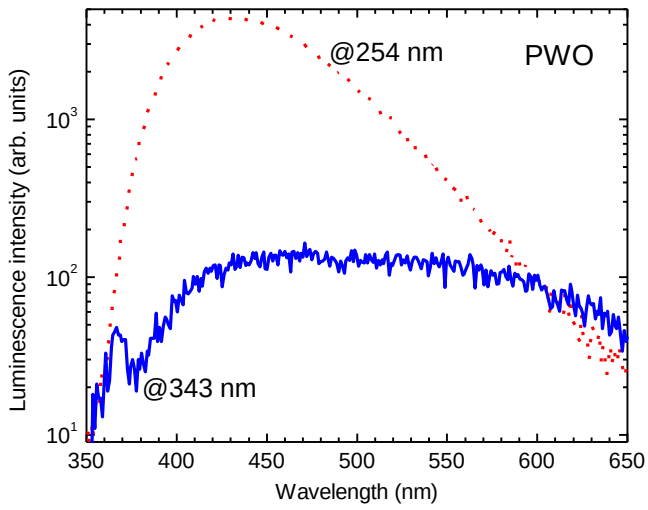

Fig. 2. Time-integrated $PbWO_4$ luminescence spectra after excitation at 254 nm (red dotted line) and 343 nm (blue solid line). Color version available online.

The PL intensity decay proceeds approximately at the same rate for all wavelengths within the PL band. The initial part in the kinetics of the PL intensity spectrally integrated within the entire band (400-600 nm) is presented in Fig. 3 together with the instrumental response function and the fit with the bi-exponential

decay function. The full width at half maximum (FWHM) of the instrumental function was 2.95 ps. The measured PL rise is completely defined by the rise of the instrumental response function. This evidences that the PL rise time in PWO scintillation crystals is in subpicosecond domain.

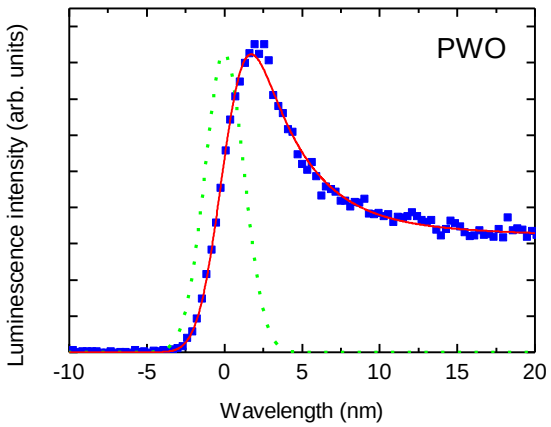

Fig. 3. Initial stage of spectrally integrated photoluminescence kinetics in $PbWO_4$ at 253 nm excitation (dots), the instrumental response function (green dotted line), and the best fit obtained using a bi-exponential decay function (red solid line). Color version available online.

It is interesting to note that both regular WO_4^{2-} and defect-related WO_3 luminescence centers show the same leading edge of the luminescence transient. This is an indication that no intermediate recapturing processes are involved in the energy transfer processes. Figure 4 shows the initial stage of PL decay. The decay has two decay components. Fitting the experimental PL transients with a bi-exponential decay function renders two effective decay times of τ_1 = 3.8 ps and τ_2 = 683 ps at 343 nm excitation and τ_1 = 5.9 and τ_2 = 824 ps, at 254 nm excitation. At the tail part of the measured kinetics curve, certain contribution of the slower component with the time constant of 8-10 ns, which is observed in routine start–stop measurements of PWO luminescence kinetics, might be traced. The intermediate component with decay times of approximately 700-800 ps is consistent with that reported in [19], while the fast component has not been observed before. The comparison of the PL transients measured at different excitation intensities (see Fig. 4) shows that the ratio between the two components does not depend on the density of the nonequilibrium carriers. The kinetics at 343 nm excitation was also measured in two spectral ranges: 400-500 and 500-600 nm. We did not find a significant difference in the response shape when intensities of blue and green luminescence bands became roughly the same. This is an

indication that the fastest decay component is due to green luminescence emitting centers.

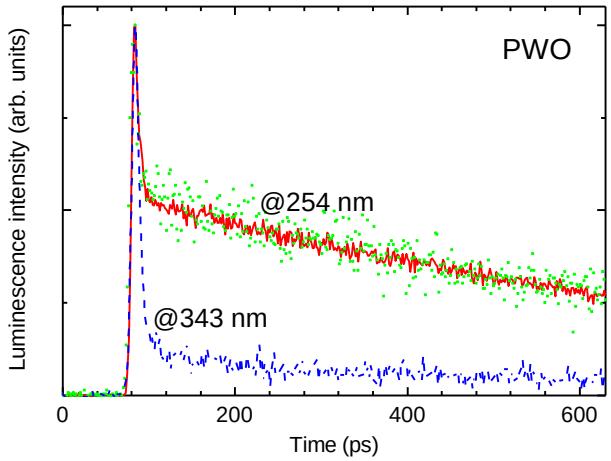

Fig. 4. Initial part of $PbWO_4$ photoluminescence kinetics at 343 nm excitation (blue dashed line) and 254 nm excitation with pulse energy of 15 mJ/cm^2 (red solid line) and 1.5 mJ/cm^2 (green dotted line). Color version available online.

3.2 Kinetics of photoluminescence in Ce-doped GAGG

Figure 5 shows the transmission and absorption spectra of GAGG:Ce crystal at room temperature. In UV-visible range, they are formed by $4f^15d^0 \rightarrow 4f^05d^1$ interconfiguration transitions of Ce^{3+} ions and $^8S \rightarrow {}^6P$, ^6I, ^6D intraconfiguration transition of Gd^{3+} ions. Gd^{3+} is the matrix creating ion, so P, I and D states form narrow subzones. The photons of 254 nm wavelength excite both Ce^{3+} and Gd^{3+} subsystems in the crystal, whereas 343 nm photons excite predominantly Ce^{3+} ions.

The photoluminescence spectra of GAGG:Ce are presented in Fig. 6. The shape of the spectra is similar for both excitation wavelengths. In consistency with the published data [16], the spectra consist of two strongly overlapping bands caused by spin-orbit splitting of ground **f** level. Meanwhile, the emission intensity under matrix excitation (at 254 nm) is by two orders of magnitude lower than that under direct excitation of Ce ions (at 343 nm). Since the absorption coefficient is similar for the two wavelengths (see Fig. 5), it seems that the difference in PL intensity is caused by the losses of the nonequilibrium carriers due to nonradiative recombination in the process of carrier transfer from the matrix to the Ce ions.

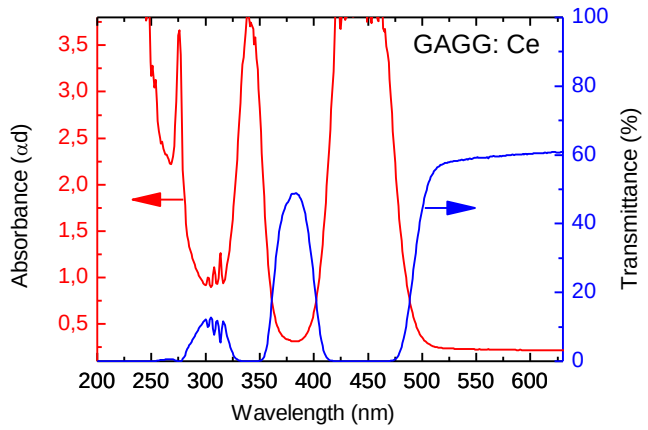

Fig. 5. Room temperature transmittance (blue) and absorption (red) spectra of GAGG:Ce sample. Color version available online.

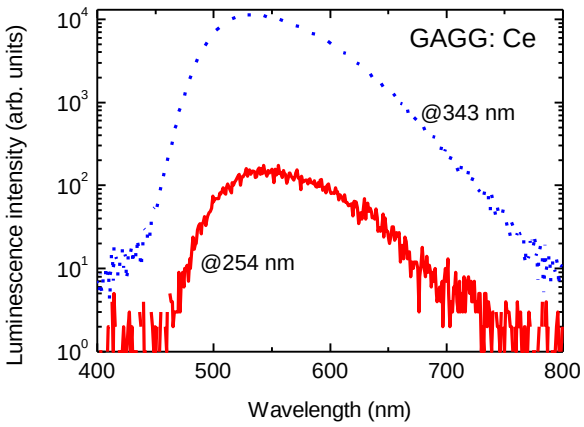

Fig. 6. Photoluminescence spectra of GAGG:Ce after short-pulse excitation at 254 nm (red solid line) and 343 nm (blue dotted line). Color version available online.

The photo-luminescence response after a short pulse excitation at 254 nm and 343 nm is presented in Fig. 7. Due to the presence of long PL decay components, the initial part of the response is measured at the instrumental function with the FWHM of 100 ps, which is, however, considerably shorter than any components in the rise of PL response in GAGG:Ce. The response was deconvoluted by taking into account the instrumental response function, an exponential rise with time constant τ_r and an exponential decay with time constant τ_d. The major part of the luminescence follows the leading edge of the instrumental function. However, at the excitation of Ce^{3+} luminescence through the matrix (at 254 nm), a slow rise with time constant τ_r = 8 ns is observed. For the 343 nm excitation corresponding to the absorption band of Ce^{3+}

ions, the slow rise component has a shorter time constant τ_r = 2.5 ns, but still considerably longer than the instrumental response function. This is in consistence with the 2 ns rise time observed in GAGG:Ce under gamma irradiation [20].

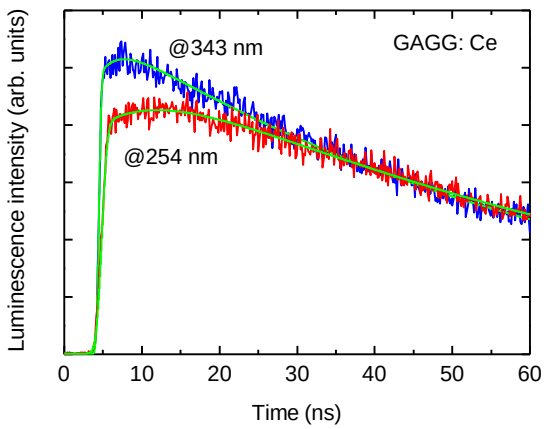

Fig. 7. The initial part of PL response to a short excitation pulse after excitation directly to Ce^{3+} ions at 343 nm and via the matrix of GAGG single crystal at 254 nm (indicated). Smooth lines represent the fitting functions. Color version available online.

Figure 8 presents the PL kinetics in a longer scale obtained at the two excitation wavelengths. The decay is mono-exponential with the decay times of 70 and 60 ns at 254 nm and 343 nm excitation wavelengths, respectively. The slightly longer decay time at excitation through the matrix might be explained by the process of Ce^{3+} luminescence sensitization [21].

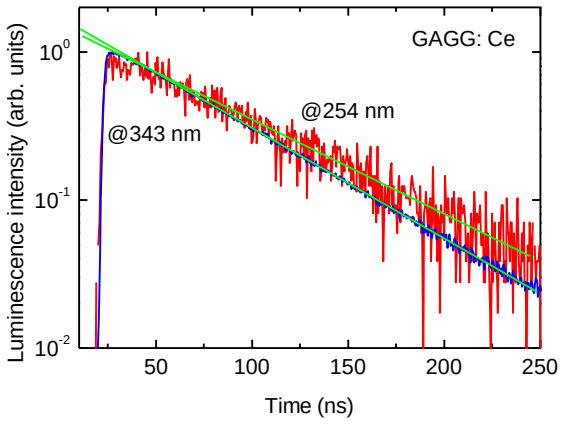

Fig. 8. Luminescence kinetics of Ce^{3+} at excitation directly to cerium ion at 343 nm and via the matrix of GAGG at 254 nm (indicated). Straight lines represent single

exponential fits. Color version available online.

3.3 Thermally stimulated luminesce in GAGG:Ce

Excitation of the GAGG:Ce crystal in the Ce^{3+}-related absorption bands results not only in the fast (ns) photoluminescence of Ce^{3+} but also in strong phosphorescence due to effective formation of stable electron and hole centers. These centers can be detected by TSL. As seen from Fig. 9, the TSL glow curves measured after irradiation of the GAGG:Ce crystal with different energies E_{irr} are similar.

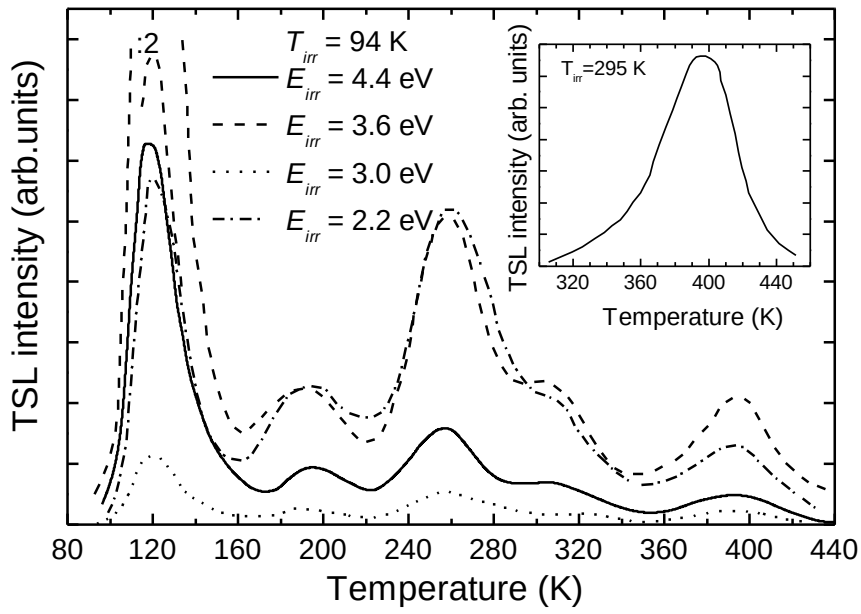

Fig. 9. Glow curves of thermally stimulated luminescence measured after irradiation of GAGG:Ce crystal at 94 K with photons of different energies E_{irr} indicated. In the inset, the TSL glow curve measured after irradiation with E_{irr} = 3.6 eV at 295 K. Color version available online.

After irradiation at 94 K, the TSL glow curve peaks located at 110, 190, 260, 310, and 395 K are observed. Most of the low temperature bands were described in detail elswhere [22-24]. After irradiation at 295 K, we observe a peak at 395 K (see the inset in Fig. 9). The resolved TSL peak above room temperature is detected for the first time. All the TSL peaks are observed for the Ce^{3+}-related emission peaked at 2.25 eV. This is an indication that all the TSL glow peaks are caused by thermally

stimulated release of electrons from different electron traps and their subsequent recombination with the hole Ce^{4+} centers.

The dependences of the maximum TSL intensity at 395 K on the irradiation energy E_{irr} measured at T_{irr} = 94 K and T_{irr} = 295 K are presented in Figs. 10a and 10b, respectively (points). For comparison, excitation spectra of the Ce^{3+} emission, measured at exactly the same conditions, are also shown (solid lines). We observed that the excitation band consist of two overlapping bands. Only one of them, corresponding to 460 nm (2.7 eV) concides with the absorption band related to Ce^{3+}, as seen in Fig. 5.

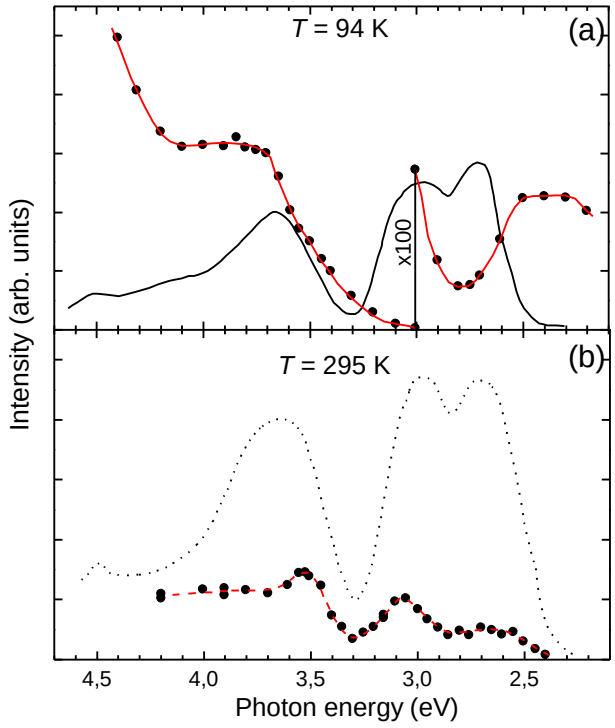

Fig. 10. Dependences of the maximum TSL intensity at 395 K on irradiation energy (points) and PL excitation spectra of the Ce^{3+} luminescence (lines) measured at irradiation temperatures of 94 K (a) and 295 K (b). Color version available online.

4. Discussion

4.1 On PWO results

The subpicosecond rise time of luminescence in lead tungstate is a clear indication that the relaxation of nonequilibrium carriers to recombination centers is an intrinsic process and is not significantly affected by any defects in a standard PWO II crystal. The short rise time at the excitation with photon energy of 4.9 eV (254 nm), which is larger than E_g by 0.6 eV [12], is consistent with the model of relaxation of germinal carrier pairs to the radiating states at oxy-complexes WO_4^{2-}. However, the fast rise time is observed also at excitation with energy 3.64 eV (343 nm), which is 0.6 eV smaller than E_g. This indicates that the process of release of electrons into conduction band from shallow traps is a weak process in this crystal. This is consistent with the assumption that the color centers with a captured electron (F+ type centers) are completely unstable in $PbWO_4$ structure at room temperature [12]. The F+ centers are based on WO_3 defect oxy-complexes and most probably have ground state inside conduction band, so they appear simultaneously with excited regular oxy-anionic groups.

The fast PL decay component with the decay time τ = 4-6 ps is more pronounced at the excitation bellow E_g. Therefore, we assume that the fastest component in the luminescence kinetics is caused by radiative decay of F^+ centers. The second, intermediate decay component with the decay time τ = 600-800 ps, which was explicitly revealed in our experiments using high time resolution streak camera, might be interpreted by WO_4^{2-} luminescence originating from quenched luminescence of complexes WO_4^{2-}+RE^{3+} (RE = La^{3+} and Y^{3+}) [12]. Therefore, the intermediate decay component (600-800 ps) and the component with the decay time of 8-10 ns, originating from regular WO_4^{2-} complexes [19], provide simultaneous contributions to luminescence, which is strongly quenched at room temperature. The PWO crystals fabricated on a large scale for high energy physics applications are doped with trivalent La and Y ions at the total level of 100 ppm [12]. As a result, radiative recombination centers WO_4^{2-}+La^{3+} and WO_4^{2-}+Y^{3+} are formed with the ground states approximately 0.1 eV below the bottom of the conduction band. Therefore, in addition to the thermal quenching, they have additional nonradiative losses due to the thermal ionization to the conduction band, so their kinetics becomes shorter.

Our results are obtained under photoexcitation near the bottom of the conduction band. Under ionizing radiation, the geminal pairs might be disconnected

during the thermalization process. Nevertheless, a dramatic increase in the rise time of the scintillation pulse is not expected, since the thermalization of the nonequilibrium carriers via the emission of phonons occurs on the time scale of picoseconds or even shorter. Moreover, the energy deposit in the high energy physics experiments, when PWO crystals interact with high-energy particles with energies of hundreds of GeV, like in LHC experiments, exceeds several GeV within a time of less than 1 ns. So the density of free carriers becomes high enough to provide prompt coupling of opposite carriers for recombination. Due to this reason we do not expect substantial increase of the scintillation rise time compared to photoluminescence rise time and estimate it at the level of less than 10 ps. Thus, the rise time of the intrinsic scintillation of PWO crystals might probably be used for fast timing with PWO crystals in high energy particles detectors with optical readout.

4.2 On GAGG:Ce results

For GAGG:Ce scintillating crystals, the excitation with 4.9eV (254 nm) photons corresponds to $^8S \rightarrow {}^6D_{7/2,9/2}$ transition of Gd^{3+} ions. The edge of the conduction band has energy near 6.2 eV (200 nm) [25], so the wavelength of 254 nm corresponds to the predominant excitation of Gd^{3+} ions. The excitation with 3.64 eV (343 nm) photons corresponds to a direct excitation of cerium ions in the second Stark component of $5d^1f^0$ configuration of Ce^{3+} ions. It is worth noting that the kinetics at both excitations shows the rise component on a nanosecond scale. The rise time at the sub-band-gap excitation (4.9eV) is only by a factor of three longer than that at the direct Ce^{3+} excitation. This is an indication of a considerable exchange of electrons between the radiative Ce^{3+} centers, sub-bands created by Gd^{3+} ions, traps, and the conduction band, where they might become trapped and reach the Ce^{3+} radiative centers with certain delay. This exchange results in slowing of the PL rise time even at the excitation wavelength corresponding to intracenter excitation.

To clarify the excitation transfer process in the crystal, we analyzed the dependences of the maximum TSL intensity at 395 K on irradiation energy. We observed that the creation spectrum of recombining electron and hole centers occurs under irradiation of the crystal in the Ce^{3+}-related absorption bands located at $E_{irr} >$ 3.3 eV and originating from the second Stark component of $5d^1f^0$ configuration (the

band at 3.65 eV) and the upper electron transitions of Ce^{3+}. The population efficiency of these centers in the region of the lowest-energy absorption band of Ce^{3+} (around 2.8 eV) is substantially smaller (at least by two orders of magnitude). At 295 K, the radiative electron and hole centers are optically populated under irradiation in all the absorption bands of Ce^{3+} (Fig. 10b). These data indicate that the second Stark component of $5d^1f^0$ configuration of Ce^{3+} is located inside the conduction band, so that the excitation into of Ce^{3+} results in the ionization of Ce^{3+} even at 94 K. As a result, the hole centers Ce^{4+} and the electrons trapped at different electron traps are optically created. Their thermally stimulated recombination results in the the TSL glow curve peaks shown in Fig. 9.

The fast rise time in the Ce^{3+} luminescence kinetics at both 4.9 eV and 3.64 eV excitations indicates that Gd^{3+} ions play a significant role in the excitation transport even at Ce^{3+} intercenter excitation. After Ce^{3+} excitation into the second Stark component and subsequent ionization into conduction band, a considerable part of the electrons are captured by matrix-building Gd^{3+} ions. An important role of Gd^{3+} ions was revealed in the study of Gd_2SiO_5:Ce crystals [26]. The migration of the electrons along Gd^{3+} subsystem in the crystal slows down the rate of the electron transfer back to the Ce^{3+} ions, where they recombine radiatively.

Moreover, another, less effective process is also possible. This effect takes place at low temperatures under irradiation of the GAGG:Ce crystal in the energy range E_{irr} < 3.0 eV. Indeed, TSL peaks at the same positions but of considerably lower intensity appear even after irradiation with E_{irr} = 2.2 eV at 94 K (see Fig. 9), however the TSL intensity under this irradiation is even larger than under irradiation in the absorption band (E_{irr} = 2.8 eV) (Fig. 10a). Probably, optically initiated population of defects in this case can be explained by charge-transfer processes, analogous to those considered in [27] for Ce^{3+}-doped oxyorthosilicates, e.g., by the optically stimulated electron transfer from the valence band to various electron traps existing in the crystal.

The TSL peak corresponding to the activation temperature near 395 K is also of interest. At room temperature, this color center undergoes slow spontaneous thermal ionization and can be a source of carriers for the subsequent capture by ions Ce^{3+}. Our results lead to certain considerations on the position of the energy level of this color center in the conduction band. Since the center is partially populated at room temperature, the position should not be above ^6P level of Gd^{3+}. The activation energy for the 395 K TSL peak under irradiation in the lowest absorption band (determined

from the lnI_{TSL} dependence on $1/T_{irr}$) is about 0.33 eV. The activation energy for quencing the Ce^{3+} luminescence is reported to be equal to 0.25 eV in a sintered sample [24] and 0.36 eV in a crystal [28]. Thus, we concluded that the ground states of both the Ce^{3+} radiating level and the color center are ~0.3 eV below the bottom of the conduction band. The nature of the color center is the subject of a separate publication. In this paper, we just point out that the spontaneous electron release from this color center at room temperature does not substantially affect the luminescence kinetics. As it can be seen in Fig.8, the decay is slightly slower at the excitation through Gd^{3+} ions but the difference in the decay times is less than 20%.

While scintillation occurs in GAGG:Ce crystal under ionizing radiation, the most of the carriers will be captuded by matrix-building Gd^{3+} ions. Thus, the rise time of the scintillation is expected in the range of few ns. The relatively long rise time of the scintillation might be the limiting factor to achieve acceptably fast timing by using detectors based on GAGG:Ce, especially in PET scanners, where the energy deposit is considerably lower than that in high energy applications.

5. Conclusions

A sub-picosecond rise time of luminescence in intrinsic PWO scintillation crystal is demonstrated for both emission components: the predominant component peaked at 430 nm, which is related with the regular crystal-building oxy-anionic complexes WO_4^{2-}, and the green component (peaked near 500 nm) due to oxygen deficient oxy-complexes WO_3. Two luminescence decay components with characteristic decay times of 4-6 ps and 600-800 ps, i.e., substantially faster than the decay component with the decay time of ~10 ns, which is usually observed in PWO scintillators, are explicitly revealed for the first time.

Meanwhile, the rise of the luminescence response to short pulse in GAGG:Ce takes several nanoseconds even at the direct resonant excitation of Ce^{3+} ions. This feature is explained by the position of the excited Ce^{3+} levels in the conduction band. This conclusion is supported by the study of thermally stimulated luminescence. The importance of the capture of nonequilibrium carriers by matrix-building Gd^{3+} ions for the luminescence response time is also concluded.

The results show that the fast rise of luminescence in PWO scintillators is short enough to be exploited for the sub-10-picosecond readout, which is targeted for the future scintillator detectors, while the rise time in cerium-doped GAGG crystal

might be a limiting factor for fast timing in radiation detectors based on this scintillator. However, as recently demonstrated in [20] and references therein, the rise time of GAGG:Ce might be substantially decreased by co-doping by magnesium.

Acknowledgement

This work has been carried out in line with the targets of Crystal Clear Collaboration and supported by H2020-INFRAIA-2014-2015 project no. 654168 (AIDA-2020). Authors are grateful to COST Action TD1401 "Fast Advanced Scintillator Timing (FAST)" for support of collaboration. V.M. also acknowledges the support of the Belarus Fundamental Research Foundation. The work of S.Z. has been supported by the Institutional Research Funding IUT02-26 of the Estonian Ministry of Education and Research.

References

[1] A. Breskin, R. Voss (Eds.), The CERN large hadron collider: accelerator and experiments, CERN, Geneva, 2009.

[2] International Linear Collider Technical Design Report, Tokyo, Geneva, Chicago – 12 June 2013.

[3] W.W. Moses, Time of Flight in PET Revisited, IEEE Trans. Nucle.Sci. 50 (2003) 1325-1330.

[4] C. Fong, A.W. Dong, A.J. Hill, B.J. Boyd, C.J. Drummond, Positron annihilation lifetime spectroscopy (PALS): a probe for molecular organization in self-assembled biomimetic systems, Phys. Chem. Chem. Phys., 17 (2015) 17527-17540.

[5] D.N. ter Weele, D.R. Schaart, P. Dorenbos, Intrinsic scintillation pulse shape measurements by means of picosecond x-ray excitation for fast timing applications, Nucl. Instrum. Methods Phys. Res. A 767 (2014) 206-211.

[6] M. Kavatsyuk, D. Bremer, V. Dormenev, P. Drexler, T. Eissner, W. Erni, E. Guliyev, T. Hennino, B. Krusche, B. Lewandowski, H. Löhner, M. Moritz, R.W. Novotny, K. Peters, J. Pouthas, P. Rosier, M. Steinacher, G. Tambave, A. Wilms, On behalf of the PANDA Collaboration, Performance of the prototype of the electromagnetic calorimeter for PANDA, Nucl. Instrum. Methods Phys. Res. A 648 (2011) 77-91.

[7] M.V. Nemallapudi, S. Gundacker, P. Lecoq, E. Auffray, A. Ferri, A. Gola, C. Piemonte, Sub-100 ps coincidence time resolution for positron emission tomography with LSO:Ce codoped with Ca, Phys. Med. Biol. 60 (2015) 4635-4649.

[8] D.R. Schaart, E. Charbon, T. Frach, V. Schulz, Advances in digital SiPMs and their application in biomedical imaging, Nucl. Instrum. Methods Phys. Res. A, 809 (2016) 31-52.

[9] M. Korzhik, A. Khruchinski, P. Lecoq, The phenomenon of scintillation in solids, Nucl. Instrum. Methods Phys. Res. A, 486 (2002) 381-384.

[10] S. Gundacker, E. Auffray, K. Pauwels, P. Lecoq, Measurement of intrinsic rise times for various L(Y)SO and LuAG scintillators with a general study of prompt 460 photons to achieve 10 ps in TOF-PET, Phys. Med. Biol., 61 (2016) 2802-2837.

[11] E. Auffray, O. Buganov, M. Korjik, A. Fedorov, S. Nargelas, G. Tamulaitis, S. Tikhomirov, A. Vaitkevičius, Application of two-photon absorption in PWO scintillator for fast timing of interaction with ionizing radiation, Nucl. Instrum. Methods Phys. Res. A 804 (2015) 194-200.

[12] A. Annenkov, M. Korzhik, P. Lecoq, Lead tungstate scintillation material, Nucl. Instrum. Methods Phys. Res. A 490 (2002) 30-50.

[13] M. Nikl, Wide Band Gap Scintillation materials:Progress in the Technology and Material Undestanding, Phys. Stat.Sol.A 178 (2000) 595-620.

[14] W. Scandale, T. Talor, F. Zimmermann (eds.), Towards a Roadmap for the Upgrade of the CERN&GSI Accelerator Complexes, CERN, Geneva, 2007.

[15] K. Kamada, T. Endo, K. Tsutumi, T. Yanagida, Y. Fujimoto, A. Fukabori, A. Yoshikava, J. Pejchal, M. Nikl, Composition Engineering in Cerium Doped $(Lu,Gd)_3(Ga,Al)_5O_{12}$ Single-Crystal Scintillators, Cryst. Growth Des. 11 (2011) 4484-4490.

[16] K. Kamada, T. Yanagida, J. Pejchal, M. Nikl, T. Endo, K. Tsukumi, Y. Fujimoto, A. Fukabori, A. Yoshikava, Crystal Growth and Scintillation properties of Ce doped $Gd_3(Ga,Al)_5O_{12}$ Single Crystals, IEEE Trans. Nucl. Sci. 59 (2012) 2112-2115.

[17] J. Ueda, K. Aishima, S. Tanabe, Temperature and compositional dependence of optical and optoelectronic properties in Ce^{3+}-doped $Y_3Sc_2(Al_{1-x}\text{-}Ga_x)O_{12}$ (x=1,2,3), Opt. Mater. 35 (2013) 182-1857.

[18] B.-T. Zhang, J.-L. He, Z.-T. Jia, Y.-B. Li, S.-D. Liu, Z.-W. Wang, R.-H. Wang, X.-M. Liu, X.-T. Tao, Spectroscopy and Laser Properties of Yb-Doped $Gd_3 Al_x Ga_{5-x} O_{12}$ Crystal, Appl. Phys. Express 6 (2013) 082702.

[19] M. Nikl , P. Bohasek, E. Mihokova, M. Kobayashi, M. Ishii, Y. Usuki, V. Babin, S. Stolovich, S. Zazubovich, M. Bacci, Excitonic Emission of sheelite tungstates AWO_4 (A=Pb, Ca, Ba, Sr), J. Lumin. 87 (2000) 1136-1139.

[20] M.T. Lucchini, V. Babin, P. Bohacek, S. Gundacker, K. Kamada, M. Nikl, A. Petrosyan, A. Yoshikawa, E. Auffray, Effect of Mg^{2+} ions co-doping on timing performance and radiation tolerance of Cerium doped $Gd_3Al_2Ga_3O_{12}$ crystals, Nucl. Instrum. Methods Phys. Res. A 816 (2016) 176-183.

[21] D.L. Dexter, A Theory of Sensitized Luminescence in Solids, J. Chem. Phys. 21 (1951) 836–850.

[22] K. Brylew, W. Drozdowski, A.J. Wojtowicz, K. Kamada, A. Yoshikawa, Studies of low temperature thermoluminescence of GAGG:Ce and LuAG:Pr scintillator crystals using the $T_{max}–T_{stop}$ method, J. Lumin. 154 (2014) 452–457.

[23] M. Kitaura, A. Sato, K. Kamada, A. Ohnishi, M. Sasaki, Phosphorescence of Ce-doped $Gd_3Al_2Ga_3O_{12}$ crystals studied using luminescence spectroscopy, J. Appl. Spectrosc. 115 (2014) 08351.

[24] E. Mihóková, K. Vávru, K. Kamada, V. Babin, A. Yoshikawa, M. Nikl, Deep trapping states in cerium doped $(Lu,Y,Gd)_3(Ga,Al)_5O_{12}$ single crystal scintillators, Radiat. Meas. 56 (2013) 98-101.

[25] J.M. Ogieglo, Luminescence and Energy Transfer in Garnet Scintillators, Utrecht University, Utrecht, 2012.

[26] D.M. Kondratiev, M.V. Korzhik, A.A. Fedorov, A.V. Pavlenko, Scintillation in cerium-activated gadolinium based crystals, Phys. Stat. Solidi (b) 197 (1996) 251-256.

[27] V. Laguta, M. Nikl, S. Zazubovich, Photothermally stimulated creation of electron and hole centers in Ce^{3+}-doped Y_2SiO_5 single crystals, Opt. Mater. 36 (2014) 1636-1641.

[28] P. Dorenbos, Electronic structure and optical properties of the lanthanide activated $RE_3(Al_{1-x}Ga_x)_5O_{12}$ (RE = Gd, Y, Lu) garnet compounds, J. Lumin. 134 (2013) 310-318.

Figure captions

Fig. 1. Streak camera image of PL intensity versus wavelength (horizontal) and time (vertical) in $PbWO_4$. Color version available online.

Fig. 2. Time-integrated $PbWO_4$ luminescence spectra after excitation at 254 nm (red dotted line) and 343 nm (blue solid line). Color version available online.

Fig. 3. Initial stage of spectrally integrated photoluminescence kinetics in $PbWO_4$ at 254 nm excitation (dots), the instrumental response function (green dotted line), and the best fit obtained using a bi-exponential decay function (red solid line). Color version available online.

Fig. 4. Initial part of $PbWO_4$ photoluminescence kinetics at 343 nm excitation (blue dashed line) and 254 nm excitation with pulse energy of 15 mJ/cm^2 (red solid line) and 1.5 mJ/cm^2 (green dotted line). Color version available online.

Fig. 5. Room temperature transmittance (blue) and absorption (red) spectra of GAGG:Ce sample. Color version available online.

Fig. 6. Photoluminescence spectra of GAGG:Ce after short-pulse excitation at 254 nm (red solid line) and 343 nm (blue dotted line). Color version available online.

Fig. 7. The initial part of PL response to a short excitation pulse after excitation directly to Ce^{3+} ions at 343 nm and via the matrix of GAGG single crystal at 254 nm (indicated). Smooth lines represent the fitting functions. Color version available online.

Fig. 8. Luminescence kinetics of Ce^{3+} at excitation directly to cerium ion at 343 nm and via the matrix of GAGG at 254 nm (indicated). Straight lines represent single exponential fits. Color version available online.

Fig. 9. Glow curves of thermally stimulated luminescence measured after irradiation of GAGG:Ce crystal at 94 K with photons of different energies E_{irr} indicated. In the inset, the TSL glow curve measured after irradiation with E_{irr}=3.6 eV at 295 K.

Fig. 10. Dependences of the maximum TSL intensity at 395 K on irradiation energy (points) and PL excitation spectra of the Ce^{3+} luminescence (lines) measured at irradiation temperatures of 94 K (a) and 295 K (b). Color version available online.